Impacts of irrigation expansion on moist-heat stress: first results from IRRMIP

Yi Yao, Agnès Ducharne, Benjamin I Cook, Steven J de Hertog, Kjetil Schanke Aas, Pedro F Arboleda-Obando, Jonathan Buzan, Jeanne Colin, Maya Costantini, Bertrand Decharme, et al.

Impacts of irrigation expansion on moist-heat stress: first results from IRRMIP

Yi Yao

yi.yao@vub.be

Vrije Universiteit Brussel https://orcid.org/0000-0003-2212-2394

Agnès Ducharne

Sorbonne Université, CNRS, EPHE, Laboratoire METIS https://orcid.org/0000-0002-6550-3413

Benjamin Cook

Lamont-Doherty Earth Observatory

Steven De Hertog

Q-ForestLab, Department of Environment, Universiteit Gent

Kjetil Aas

CICERO Center for International Climate and Environmental Research in Oslo

Pedro Arboleda-Obando

Laboratory 7619 METIS, Sorbonne Université, CNRS, EPHE, IPSL

Jonathan Buzan

University of Bern

Jeanne Colin

Centre National de Recherches Météorologiques (CNRM), Météo-France/CNRS

Maya Costantini

Centre National de Recherches Météorologiques (CNRM), Université de Toulouse

Bertrand Decharme

CNRM, Centre National de Recherches Météorologiques, Université de Toulouse, Météo-France, CNRS
https://orcid.org/0000-0002-8661-1464

David Lawrence

NSF NCAR https://orcid.org/0000-0002-2968-3023

Peter Lawrence

National Center for Atmospheric Research https://orcid.org/0000-0002-4843-4903

L. Ruby Leung

Pacific Northwest National Laboratory https://orcid.org/0000-0002-3221-9467

Min-Hui Lo

Department of Atmospheric Sciences, National Taiwan University, Taipei, Taiwan
https://orcid.org/0000-0002-8653-143X

Devaraju Narayanappa

Advanced Computing Facility Unit, CSC- IT Center for Science

William Wieder

National Center for Atmospheric Research https://orcid.org/0000-0001-7116-1985

Ren-Jie Wu

National Taiwan University

Tian Zhou

Atmospheric, Climate, and Earth Sciences Division, Pacific Northwest National Laboratory

Jonas Jaegermeyr

Columbia University https://orcid.org/0000-0002-8368-0018

Sonali McDermid

New York University https://orcid.org/0000-0002-4244-772X

Yadu Pokhrel

Department of Civil and Environmental Engineering, Michigan State University

Maxwell Elling

NASA Goddard Institute for Space Studies https://orcid.org/0000-0001-6091-809X

Naota Hanasaki

National Institute for Environmental Studies https://orcid.org/0000-0002-5092-7563

Paul Muñoz

Vrije Universiteit Brussel https://orcid.org/0000-0002-8000-8840

Larissa Nazarenko

Kedar Otta

National Institute for Environmental Studies

Yusuke Satoh

Korea Advanced Institute of Science and Technology

Tokuta Yokohata

National Institute for Environmental Studies https://orcid.org/0000-0001-7346-7988

Lei Jin

Sino-French Institute for Earth System Science, College of Urban and Environmental Sciences, Peking University

Xuhui Wang

Peking University https://orcid.org/0000-0003-0818-9816

Vimal Mishra

Indian Institute of Technology Gandhinagar https://orcid.org/0000-0002-3046-6296

Subimal Ghosh

Indian Institute of Technology Bombay

Wim Thiery

Vrije Universiteit Brussel https://orcid.org/0000-0002-5183-6145

Article

Keywords:

Posted Date: September 4th, 2024

DOI: https://doi.org/10.21203/rs.3.rs-4835411/v1

Additional Declarations: There is **NO** Competing Interest.

Impacts of irrigation expansion on moist-heat stress: first results from IRRMIP

Yi Yao *[1], Agnès Ducharne[2], Benjamin I Cook[3], Steven J. De Hertog[4,1], Kjetil Schanke Aas[5], Pedro F. Arboleda-Obando[2], Jonathan Buzan[6,7], Jeanne Colin[8], Maya Costantini[8], Bertrand Decharme[8], David M. Lawrence[9], Peter Lawrence[9], L. Ruby Leung[10], Min-Hui Lo[11], Devaraju Narayanappa[12], Will Wieder[9], Ren-Jie Wu[11], Tian Zhou[10], Jonas Jägermeyr[13, 14, 15], Sonali McDermid[3], Yadu Pokhrel[16], Maxwell Elling[14], Naota Hanasaki[17], Paul Muñoz[1], Larissa Nazarenko[3], Kedar Otta[17], Yusuke Satoh[18], Tokuta Yokohata[17], Lei Jin[19], Xuhui Wang[19], Vimal Mishra[20, 21], Subimal Ghosh[22], Wim Thiery[1]

[1]Department of Water and Climate, Vrije Universiteit Brussel, Brussels, Belgium
[2]Laboratory 7619 METIS, Sorbonne Université, CNRS, EPHE, IPSL, Paris, France
[3]Department of Environmental Studies, New York University, New York, NY, USA
[4]Q-ForestLab, Department of Environment, Universiteit Gent, Ghent, Belgium
[5]CICERO Center for International Climate and Environmental Research in Oslo, Oslo, Norway
[6]Climate and Environmental Physics, Physics Institute, University of Bern, Bern, Switzerland
[7]Oeschger Centre for Climate Change Research, University of Bern, Bern Switzerland
[8]Centre National de Recherches Météorologiques (CNRM), Université de Toulouse, Météo-France, Toulouse, France
[9]Climate and Global Dynamics Laboratory, National Center for Atmospheric Research, Boulder, USA
[10]Atmospheric, Climate, and Earth Sciences Division, Pacific Northwest National Laboratory, Richland, WA, USA
[11]Department of Atmospheric Sciences, National Taiwan University, Taipei, Taiwan
[12]Advanced Computing Facility Unit, CSC- IT Center for Science, Espoo, Finland
[13]Columbia University, Climate School, New York, NY 10025, USA
[14]NASA Goddard Institute for Space Studies, New York, NY 10025, USA
[15]Potsdam Institute for Climate Impact Research (PIK), Member of the Leibniz Association, 14412, Potsdam, Germany
[16]Department of Civil and Environmental Engineering, Michigan State University, East Lansing, MI, USA
[17]National Institute for Environmental Studies, Tsukuba, 305-8506, Japan
[18]Moon Soul Graduate School of Future Strategy, Korea Advanced Institute of Science and

Technology, Daejeon, Republic of Korea
[19]Sino-French Institute for Earth System Science, College of Urban and Environmental Sciences, Peking University, Beijing, China
[20]Civil Engineering, Indian Institute of Technology (IIT), Gandhinagar, India
[21]Earth Sciences, Indian Institute of Technology (IIT), Gandhinagar, India
[22]Interdisciplinary Program in Climate Studies, Indian Institute of Technology Bombay, Mumbai, India

Irrigation rapidly expanded during the 20th century, thereby affecting climate via changes in water, energy, and biogeochemical cycling. Previous assessments of these historical climate effects of irrigation expansion predominantly relied on a single Earth System Model, and therefore suffered from structural model uncertainties. Here we quantify the impacts of historical irrigation expansion on climate by analysing simulation results from six Earth system models participating in the Irrigation Model Intercomparison Project (IRRMIP). Despite the large range of simulated irrigation water withdrawal from those models (∼900 to ∼4000 km^3 after the year 2000), our results show that irrigation expansion causes a rapid increase in irrigation water withdrawal, which leads to less frequent 2-meter air temperature heat extremes across heavily irrigated areas (≥4 times less likely). However, due to the irrigation-induced increase in air humidity, the cooling effect of irrigation expansion on moist-heat stress is less pronounced or even reversed, depending on the heat stress metric. In summary, this study suggests the priorities in irrigation dataset collection and parameterisation development, and shows that irrigation deployment is not an efficient adaptation measure to escalating human heat stress under climate change, calling for carefully dealing with the increased exposure of local people to moist-heat stress.

Irrigation increases crop yield and currently accounts for more than 70 % of total human freshwater use[1]. Irrigation-related water withdrawal and application have substantial impacts on global and regional water, energy, and biogeochemical cycles[2–5], and therefore can change the magnitude and pattern of some meteorological conditions[6–8]. Notably, irrigation has a cooling effect on near-surface temperature[9–11], especially during hot extremes[12,13]. For that reason, irrigation has been proposed as a potential land management strategy for balancing extreme heat escalation under anthropogenic climate change[13–15].

Most previous studies only focused on temperature differences, ignoring that human comfort is also affected by heat dissipation[16]. Evaporative cooling is the main way humans lose heat[17], and air humidity and wind speed greatly influence evaporation efficiency[18]. These metrics can also be altered by irrigation[19,20], suggesting that irrigation-induced impacts on human comfort

*corresponding author, email: yi.yao@vub.be

during heat stress may be complex. Multiple moist-heat metrics were developed to quantify the compound effects of different meteorological conditions on heat stress[21,22], and some of them have been used in irrigation-related studies. For example, over intensely irrigated regions in India, the wet bulb temperature (T_w) was simulated to increase due to irrigation, despite a lowering of the temperature[23,24]. In addition to the ignorance of changes in air humidity, existing modelling studies generally use a static irrigated land map and rely on a single Earth System Model (ESM), which can introduce uncertainties in their results.

To address these limitations, we launched the Irrigation Model Intercomparison Project (IRRMIP) to comprehensively explore the impacts of irrigation expansion on climate and water resources during the 20^{th} century. The IRRMIP protocol consists of two transient AMIP-style[25] historical climate experiments, one with and one without irrigation expansion, during the period 1901-2014. Here we analyse IRRMIP simulations from six ESMs to study the impacts of irrigation expansion on historical (moist-)heat stress. We calculate several moist-heat metrics based on 3-hourly 2-meter air temperature (T_{2m}), 2-meter air relative humidity, and 10-meter wind speed. By comparing the results from different experiments and periods, we separate the effects of irrigation expansion and other forcings on high percentiles of these metrics. We aim at consolidating the understanding of irrigation-induced impacts on (moist-)heat stress, facilitating the inclusion of these impacts in future local land-use and land-management planning.

Irrigation expansion drives the increase in water withdrawal Global area equipped for irrigation has experienced substantial expansion from 1901 to 2014, increasing almost six-fold from 0.5×10^6 km^2 to around 3×10^6 km^2 (Figure 1a). Expansion mainly happened in some irrigation hot spots, including South Asia (SAS), East Asia (EAS), and Central North America (CNA) (Figure 2a, b). In 1901, most of the global irrigated land was concentrated over the regions where rice is the main staple food, such as India, China, and Japan (Figure A1a). Since 1901, irrigated land has risen slowly over many regions until the 1950s, followed by an accelerated increase during the second half of the century (Figure 1a). Until 2014, the irrigated areas in India and China experienced intensification and expansion, with some grid cells having a $\geq$40% (of the grid cell area) increase in irrigated area (Figure 2a, A1d). Over North America, some new densely irrigated grid cells appear in CNA, while for other regions, the expansion is limited (mostly below 10% of the grid cell area).

The spatial pattern of simulated irrigation water withdrawal (IWW) is in agreement with the distribution of the area equipped for irrigation (Figure 2c-d). India is still the most intensively irrigated region, consisting of many grid cells (0.9°x1.25°) with more than 250 mm yr^{-1} of IWW. The six IRRMIP models simulate a broad range of global IWW (900 to 4000 km^3 yr^{-1} after the year 2000), but the temporal trend of simulations with transient irrigation extent (hereafter referred to as *tranirr*) generally aligns with that of the area equipped for irrigation. Consistent with a previous review[5], simulated annual IWW during the post-2000 period ranges from $\sim$900 to $\sim$4000 km^3 yr^{-1} (Figure 1c-h), due to different representations of irrigation in these

models. CESM2, CESM2_gw, and NorESM2 show high similarity because they share the same atmosphere and land models, with comparably small differences in specific sub-models (see Supplementary Note 1).

Based on IWW and irrigated area, we select several regions, including West North America (WNA), CNA, North Central America (NCA), Mediterranean (MED), west Central Asia (WCA), SAS, EAS, and Southeast Asia (SEA) (Figure 2b), to calculate regional irrigation water quantities (Figure 1c-h). SAS is the region with the highest IWW in all models, but its relative importance varies. For example, after the year 2000, SAS accounts for around one-third of global IWW simulated by CESM2 (32.4% to 35.8%), CESM2_gw (31.4% to 35.1%), E3SM (27.5% to 41.8%), and NorESM (32.8% to 35.1%), but in IPSL-CM6, this fraction is less than one-fourth (16.0% to 20.4%). WCA consumes the second-highest quantity of IWW, even though its area equipped for irrigation is less than EAS. This indicates that simulated IWW is dependent not only on the area equipped for irrigation but also on other factors, such as background climate conditions.

Different feedback from heat and moist-heat stress to irrigation expansion Here we focus on T_{2m}, HUMIDEX (HU), and T_w warm extremes, as many other metrics are weighted average values of T_{2m} and T_w. Changes in high percentiles of these three metrics could be interpreted as the impacts of irrigation expansion and other forcings on dry heat stress (T_{2m}), human comfort (HU), and humid heat stress (T_w) (Table 1). In the *tranirr* experiment, climate change, land use change, and irrigation expansion, are all transient throughout the simulation period, so by comparing the last-30-year of *tranirr(1985-2014)* to the first-30-year of *tranirr(1901-1930)*, we can quantify the impacts of all forcings (greenhouse gas emissions, land use and land management change, irrigation expansion, etc.). Similarly, in the experiment with fixed irrigation extent (*1901irr*), the difference between the first- and the last-30-year periods (*1901irr(1901-1930)* and *1901irr(1985-2014)*) gives the impacts of all forcings minus irrigation expansion. Finally, by subtracting the outputs of *tranirr(1985-2014)* from *1901irr(1985-2014)*, we obtain the impacts of irrigation expansion. Hence, in this study, the sum of all forcings minus irrigation expansion (ALL-IE) and irrigation expansion (IE) does not exactly equal to all forcings (ALL).

Since we focus on extreme events, we first calculate the 99.9^{th} percentile values (one-in-1000 time steps warm event) of three metrics in all four exp-periods, and take the one of *1901irr(1901-1930)* as the reference (Figure 3). Several irrigation hot spots, like SAS, WCA, NCA, and CNA, are also extreme heat hot spots, with a 99.9^{th} percentile value of T_{2m} exceeding 40 °C in many grid cells. Other forcings cause a general warming signal (+0.5 to +2 °C), except in some conventional irrigation hot spots like SAS and EAS, which may be attributed to the increasing aerosol concentrations[26,27]. irrigation expansion has substantial cooling impacts in heavily irrigated grid cells (>1 °C) and weaker impacts over surrounding grid cells (<0.5 °C). This cooling effect creates regional irrigation-induced 'cooling islands' against the global warming background, like the Indo-Gangetic Plain and several grid cells in Central USA. Interestingly,

irrigation expansion's cooling impacts on the extreme value of HU are much less substantial, and mainly occur over the surrounding regions of intensely irrigated pixels. One reason for this could be that increased air humidity over these regions dominates the impacts on HU.

To quantify the changes in extreme heat events frequency, we then calculate the probability ratio (PR) of T_{2m}, HU, and T_w warm extremes between different exp-periods (Figure 4). We find that the pattern of these impacts is similar to those on the absolute value of heat extreme events (Figure 3). Other forcings, especially greenhouse gas emissions, contribute to a warmer world, with > 4 times increased frequency for the events of all three metrics in most grid cells in tropical and sub-tropical regions. Most models agree that irrigation expansion substantially reduces the frequency of T_{2m} extremes, especially in SAS, WCA, and CNA. However, its impacts on HU and T_w are much less pronounced and are also less consistent among models. Similarly, for T_w, the dampening impacts of irrigation on extreme high events disappear over the most intensely irrigated area like India and are reversed to an intensifying effect in the Central CNA and WCA, where the 99.9^{th} percentile T_w event happens more than 3 times more often due to irrigation expansion. Consistent with a previous study using the Goddard Institute for Space Studies (GISS) climate model, the frequency in moist-heat extremes does not increase in some regions with intense irrigation, like the North India and California. One reason may be the high background temperature and air humidity in this region, as (i) more water in the air is needed to increase relative humidity under a higher temperature; and (ii) more extra relative humidity is needed to increase T_w when the relative humidity is higher[28]. In India, another reason may be the temporal mismatch between the irrigation activities and moist-heat extremes, as indicated by a previous study[29].

The more extreme the T_{2m} heat events are, the more pronounced irrigation expansion-induced impacts become (Figure A2). The impacts of irrigation expansion on T_{2m} are mainly limited to irrigation hot spots for the 99^{th} percentile heat event, e.g., large changes in PR (that is, $>$ 2 times less likely) are only found in North India and Central USA. When the events get more extreme (99.5^{th} percentile and 99.9^{th} percentile), the affected areas expand around these hot spots and also appear in other regions like Europe and East China. The slight cooling impacts on HU and warming effects on T_w are also more pronounced when events get more extreme (Figure A3 and A4). Interestingly, in a previous study based on GISS model simulations[30], the heat extremes of equivalent temperature are widely increased in many regions, indicating the importance of considering different metrics, so we also calculate irrigation expansion's impacts on other moist-heat metrics (Figure A5). We find that the significance of irrigation expansion's impacts on the apparent temperature is similar to HU, and as for other moist-heat metrics, the magnitude and consistency depend on the weight of T_w and T_{2m}.

We calculate the average annual hours (weighted by areas) exposed to extreme events of the grid cells with more than 40% (of the grid area) irrigation expansion (Figure 5). The average

annual hours exposed to T_{2m} extreme events show a slight increase in the first half of the century, then increases rapidly between 1950 and 1980, and keeps steady in the last decades. Irrigation expansion causes a decreasing trend in the hours exposed to heat extremes in heavily irrigated regions, in spite of global warming. However, for HU, the cooling impacts of irrigation expansion are quite small, thus the hours exposed to extreme HU events still increase, but at a slightly slower speed than those without irrigation expansion. Interestingly, the hours exposed to T_w extreme events for both *1901irr* and *tranirr* remain almost unchanged until 1980. After 1980, this starts to rise rapidly. In the case of *tranirr*, the hours are slightly higher than 1901irr, indicating the intensifying impact of irrigation expansion over these grid cells. Since T_{2m} extremes are the most substantially affected events, we also calculate the average annual hours exposed to different magnitude of T_{2m} extreme events (the 99.0^{th}, the 99.5^{th} and the 99.9^{th} percentile events) over different groups of grid cells (with 0%-20%, 20%-30%, 30%-40%, and more than 40% of irrigation expansion) (Figure A8). Despite the difference in magnitudes, irrigation expansion has similar reducing impacts on all degrees of T_{2m} extreme events, which become more substantial with the extent of irrigation expansion.

Limited irrigation expansion-induced impacts on radiation fluxes Changes in surface energy fluxes may induce changes in temperature. However, the impact of irrigation on some energy fluxes, especially up/downwelling short/longwave radiation, still lacks consistency across model simulations[7,10,31–33]. It is known that irrigation practices enhance evapotranspiration processes, contributing to wetter air. As a result, irrigation expansion increases latent heat flux (LHF) and decreases sensible heat flux (SHF), especially in irrigation expansion hot spots (Figure A6). The impact on LHF is slightly larger than on SHF both in magnitude and range. The effects on net radiation (Rnet) are smaller and less consistent among models, but in SAS, WCA, and CNA, most models agree that irrigation expansion increases Rnet. The IRRMIP models show little agreement in the magnitude and even sign of the change of the surface radiation components in response to irrigation expansion, except for upwelling longwave radiation (LWup) (Figure A7). A decrease in LWup caused by irrigation expansion could be linked to the decrease in surface temperature, which then results in an increase in Rnet.

Discussion Six ESMs simulate a broad range of IWW ($\sim$900 to $\sim$4000 $km^3\,yr^{-1}$ after the year 2000) with a median value of around 1500 $km^3\,yr^{-1}$ (Figure 1), which is lower than the value of 2761 $km^3\,yr^{-1}$ reported for the period 2005-2007[34]. Most models, especially those which have CLM5 as their land model, substantially underestimate the global IWW, which could be attributed to its over-conservative irrigation water demand calculation[31]. A new modification has been made by implementing different irrigation techniques[31], in which the non-effective water consumption is more comprehensively considered, outperforming substantially compared to the original module at global or regional levels. In E3SM a slightly higher IWW is simulated, possibly due to the higher spatial resolution and its added features like surface/groundwater demand separation[35], and an interactive surface water withdrawal module[36]. The overestimation

of CNRM-CM6-1 originates from an external dataset reconstructed with a global hydrological model[37], in which the irrigation water abstraction from groundwater is not limited by water resources[38]. In IPSL-CM6[39], a constraint is imposed on IWW based on the water availability, with the parameters sensitivity tests and calibratio, showing a superior performance of reproducing global IWW despite the slight underestimation. Overall, the implementation of irrigation techniques, groundwater withdrawal, water resources management, water availability, and the calibration and validation of irrigation-related parameters, should all be considered in the next generation of irrigation representations in ESMs.

Despite the wide range of simulated IWW, ESMs used in this study agree that irrigation has a cooling impact on local hot extremes, which is consistent with previous studies[10,13,14]. This cooling impact has the potential of mitigating the heat exposure of both local inhabitants and crops[40]. However, reduced temperature does not decrease the frequency of moist-heat stress by a similar magnitude, and most ESMs even believe that historical irrigation expansion has an intensifying impacts on T_w extremes in some regions like the Central USA and West Asia (Figure 3), possibly endangering local population. Many moist-heat metrics are calculated in this study, and the impacts of irrigation expansion on extreme events of those metrics vary A5, mainly depending on the relative contribution of air humidity and temperature. Generally, the more important role temperature plays, the more substantial cooling impact of irrigation expansion is found.

Similar to previous ESM-based impact studies regarding moist-heat metrics[41,42], we use temperature, moisture, and wind speed at the grid-cell level which are averaged based on values from different land cover tiles. Thus, coarse-resolution simulations' suitability to calculate human heat metrics may be questionable, as sub-grid scale extreme values could be masked. Constrained by computational resources, conducting long-term high-resolution global simulations at less than 100 km resolution is very expensive. However, those simulations at coarser resolution remain important for understanding the spatial distribution and temporal trend of irrigation-induced impacts on moist-heat stress.

In summary, our study stresses an over-optimism regarding irrigation's health benefits, which ignores the impacts of increased air humidity on human comfort. Different metrics extremes have various feedback to irrigation expansion, highlighting the importance of better understand the most suitable metrics for people with different races, genders, ages, health conditions, etc. As a metric commonly used in outdoor activities guidance, T_w extreme events are even intensified by irrigation expansion in some regions. Under global warming scenarios, intolerable T_w events will occur more frequently, especially in SAS, CNA, and EAS[43]. Even more troublesome, the maximum T_w is tied to atmospheric buoyancy, which is determined by global mean surface temperatures[45,46]. T_w will increase to the new irrigated value, and scale with global mean temperature changes[17]. This calls for better monitoring of local moist-heat metrics to inform

exposed communities of the potential danger, and the exploration of potential solutions.

Acknowledgements Y.Y. holds a China Scholarship Council (CSC) Studentship with Vrije Universiteit Brussel. W.T. acknowledges funding from the European Research Council (ERC) under the European Union's Horizon Framework research and innovation programme (grant agreement No 101076909; 'LACRIMA' project). The computational resources and services used in this work for the simulations and storage of CESM data were provided by the VSC (Flemish Supercomputer Center), funded by the Research Foundation - Flanders (FWO) and the Flemish Government – department EWI. A.D. and P.A.O. got support from the Belmont Forum (project BLUEGEM, grant no. ANR-21-SOIL-0001), and their simulations were done using the IDRIS computational facilities (Institut du Développement et des Ressources en Informatique Scientifique, CNRS, France), S.D.H. acknowledges funding by BELSPO (B2/223/P1/DAMOCO). L.R.L. and T.Z. are supported by Office of Science, U.S. Department of Energy (DOE) Biological and Environmental Research through the Water Cycle and Climate Extremes Modeling (WACCEM) scientific focus area funded by the Regional and Global Model Analysis program area. Pacific Northwest National Laboratory is operated for DOE by Battelle Memorial Institute under contract DE-AC05-76RL01830. NorESM simulations were performed using Computational Resources from the NN8057K project provided by Sigma2— the National Infrastructure for High-Performance Computing and Data Storage in Norway. Y.P. received support from the National Science Foundation (Belmont Forum project BLUEGEM; Award #: 2127643).

Author Contributions Y.Y. and W.T. designed the study and coordinated IRRMIP. Y.Y. wrote the manuscript with support from all authors and performed all analyses under the supervision of W.T. The IRRMIP simulations were performed by Y. Y., S. D. H., P. L., D. M. L., W. W. for the CESM2 model, by R. W., M. L., and Y. P. for the CESM2_gw model, by D. N., K. S. A., M. B. for the NorESM model, by T. Z., L. R. L. for the E3SM model, by P. A. O. and A. D. for IPSL-CM6 model, by J. C. and B. D. for CNRM-CM6-1 model. J. B. provided guidance on the calculation of heat metrics.

Competing Interests The authors declare no Competing Interests.

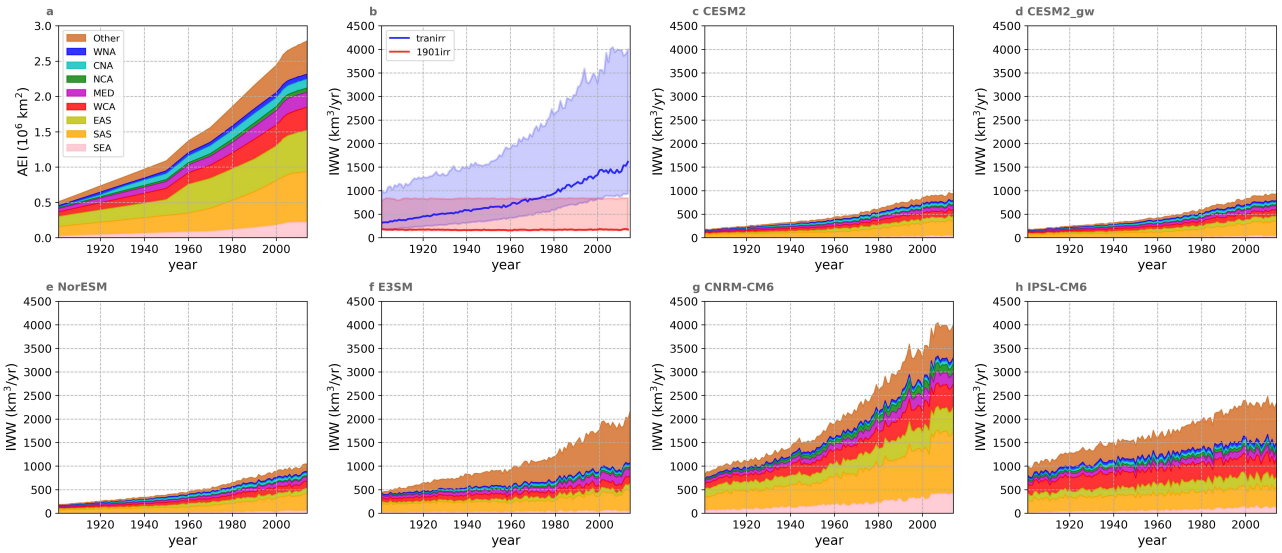

Figure 1: **Historical increase in area equipped for irrigation and simulated irrigation water withdrawal. a** Global and regional time series of area equipped for irrigation (AEI) in 1901-2014. The area equipped for irrigation data is from the Land-Use Harmonization phase 2 (LUH2) project[47], and the grid cells corresponding to IPCC reference regions are indicated in Figure 2b. **b** Simulated mean global irrigation water withdrawal (IWW) with (blue: *tranirr*) and without (red: *1901irr*) irrigation expansion by all six models. The line indicates the median value of six models and the range indicates the maximum and minimum values. Note that IWW of CNRM-CM6-1 is applied as an external input, which is the irrigation fluxes from a global reconstructed hydrological dataset based on simulations[37]., and for the *1901irr* experiment of IPSL-CM6, irrigation is switched off. **c-h** Global and regional IWW simulated by CESM2 (**c**), CESM2_gw (**d**), NorESM (**e**), E3SM (**f**), CNRM-CM6-1 (**g**) and IPSL-CM6 (**h**).

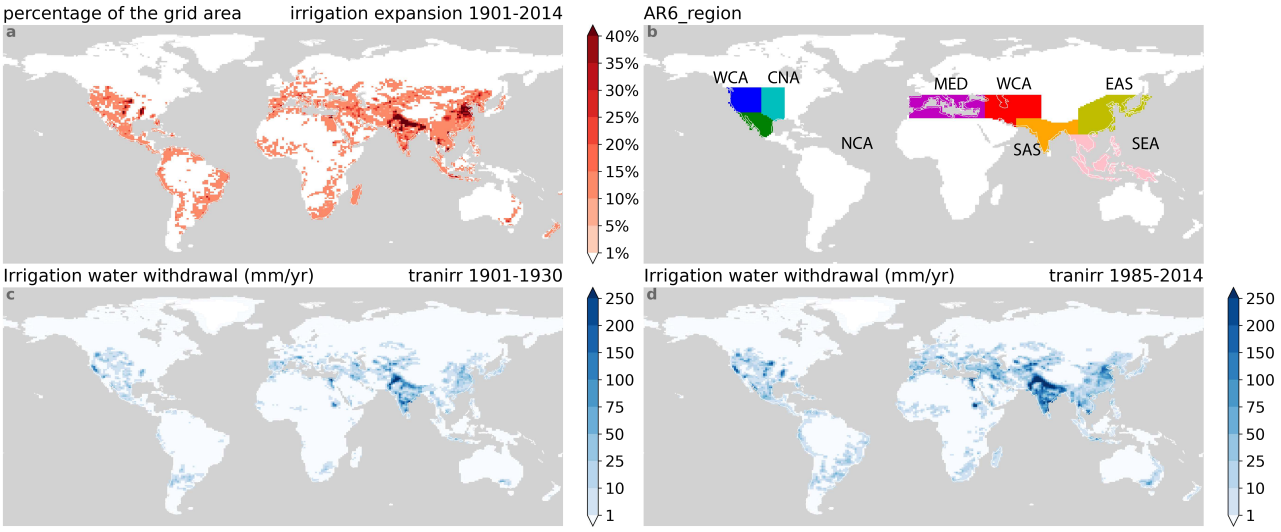

Figure 2: **Spatial pattern of irrigation expansion and simulated irrigation water withdrawal in different periods. a** Increase in irrigated fraction between 1901 and 2014. **b** Grid cells of the IPCC reference regions[48] used in the analysis. The grid resolution is the simulation resolution of CESM2, CESM2_gw, and NorESM (0.9° x 1.25°). **c-d** Multi-model mean simulated annual IWW with transient irrigation (tranirr) extent during the first 30 years (1901-1930: **c**) and the last 30 years (1985-2014: **d**)

Figure Legends/Captions

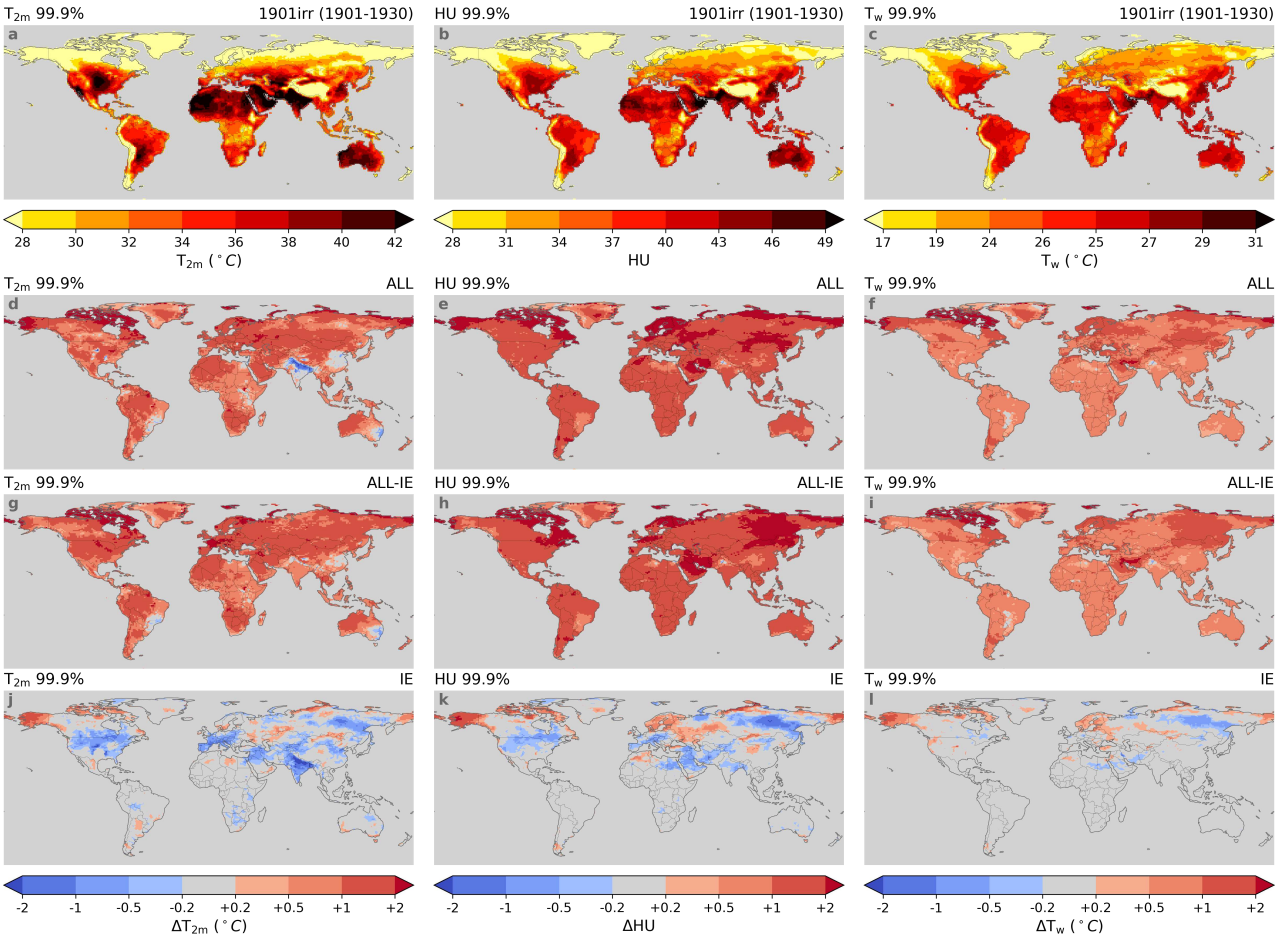

Figure 3: **Heat and moist-heat extremes and impacts of different forcings on them. a-c** Multi-model mean absolute values of the 99.9th percentile values of 2-meter air temperature (T_{2m}: **a**), HUMIDEX (HU: **b**), and wet-bulb temperature (T_w: **c**) of the first 30 years (1901-1930) in the simulations without irrigation expansion (*1901irr*). **d-l** Multi-model mean impacts of all forcings (ALL: greenhouse gas emissions, land use and land management change, irrigation expansion, etc.) (**d, e, f**), all forcings except irrigation expansion (ALL-IE: **g, h, i**), and irrigation expansion (IE: **j, k, l**) on the 99.9th percentile values of T_{2m} (**d, g, j**), HU (**e, h, k**), and T_w (**f, i, l**). Impacts are calculated by subtracting the values in the new exp_period by those in the reference exp_period (see Table 1). Only signals (>0.2 or <-0.2) agreed by $\geq$ 4 of 6 models are shown.

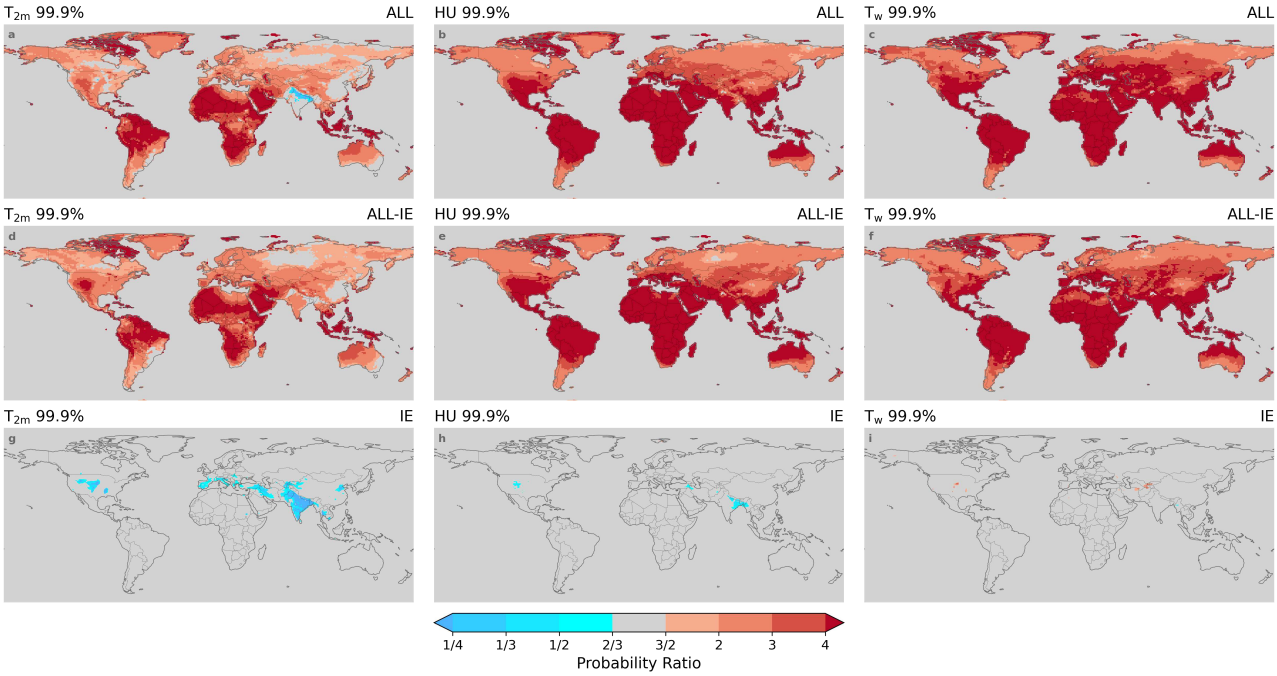

Figure 4: **Changes in the frequency of (moist-)heat extreme events induced by different forcings. a-i** Impacts of all forcings (ALL: **a, b, c**), all forcings except irrigation expansion (ALL-IE: **d, e, f**), and irrigation expansion (IE) on the frequency of the events in which 2-meter air temperature (T_{2m}: **a, d, g**), HUMIDEX (HU: **b, e, h**), and wet bulb temperature (T_w: **c, f, i**) exceed their 99.9th percentile values of the first 30 years (1901-1930) in the simulations without irrigation expansion (*1901irr*) shown in Figure 3**a-c**. Impacts are quantified by probability ratio (PR) which is calculated by dividing the events frequencies in the new exp_period by those in the reference exp_period (see Table 1), and the values are the sixth root of the product of PR calculated from the outputs of six ESMs. Only signals (>3/2 or <1/2) agreed by $\geq$ 4 of 6 models are shown.

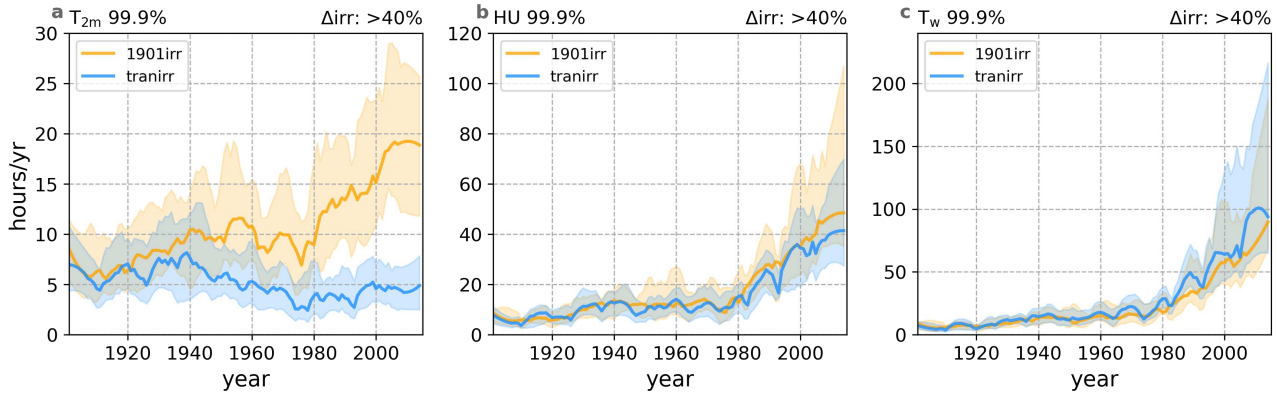

Figure 5: **Increase in annual hours exposed to (moist-)heat extreme events over the grid cells with the most substantial irrigation expansion. a-c** Time series of the annual hours over the grid cells with $\geq$ 40% of irrigated fraction increase (in the year 2014 compared to the year 1901) of 2-meter air temperature (T_{2m}: **a**), HUMIDEX (**b**), and wet bulb temperature (T_w: **c**) warm extremes. The warm extremes are defined as the period when T_{2m}, HU, and T_w exceed their 99.9th percentile values of the first 30 years (1901-1930) in the simulations without irrigation expansion (*1901irr*). Lines indicate the median value among six models and ranges indicate the middle four of six models. Curves were smoothed using Savitzky-Golay filtering (order = 2, window = 15)[49]. The range of the y-axes are different for three sub-plots.

Table 1: Approach to separate the impacts of different forcings

Reference exp_period	New exp_period	Forcings
tranirr_1901-1930	tranirr_1985-2014	all forcings (greenhouse gas emissions, land use change, irrigation expansion, etc.)
1901irr_1901-1930	1901irr_1985-2014	all forcings except irrigation expansion
1901irr_1985-2014	tranirr_1985-2014	irrigation expansion

Methods

Participating ESMs and simulation protocol Six combinations of state-of-art Earth system models (ESMs) and irrigation parametrizations are used in this study: the Community Earth System Model version 2 (CESM2)[50], CESM2 with groundwater withdrawal and flow representation (CESM2_gw)[8], the Institut Pierre-Simon Laplace Climate Model version 6 (IPSL-CM6)[51] with a newly developed irrigation scheme[39], the Norwegian Earth System Model version 2 (NorESM2)[52], the Energy Exascale Earth System Model Version 2 (E3SMv2)[53] with active two-way coupled irrigation scheme[36], and the Centre National de Recherches Météorologiques Climate Model version 6 (CNRM-CM6-1)[54,55]. Irrigation is represented in different ways in these models, which can be divided into two categories: soil-moisture-based schemes and external forcing applications (only for CNRM-CM6-1). Differences between soil-moisture-based irrigation modules relate to irrigation triggers, start time, duration, amount, and the method of water application. The employed ESMs provide the option to customise irrigation-related parameters, but in this study, all ESMs used default parameter values. CESM2, CESM2_gw, and NorESM2, share identical or similar land system models, which explains why they show strong consistency between each other. However, their differences in atmospheric models and features in the irrigation scheme, still represent an added value to this study. More detailed description of ESMs and their irrigation representations could be found in Supplementary Note 1.

We design two historical experiments in this study: with (*tranirr*) and without (*1901irr*) historical irrigation expansion. The simulations of both experiments follow the protocol of AMIP simulations in CMIP6 with the same input data[56], which means that the ocean model is switched off and sea surface temperatures are prescribed. To better capture the signal of irrigation extent increase in the 20$^{\text{th}}$ century, we select a simulation period of 1901 - 2014. The only difference between the two experiments is that in *tranirr*, irrigation extent is transient, while in *1901irr*, the irrigation extent is fixed at the level in the year 1901. One exception is IPSL-CM6, where irrigation is entirely switched off for *1901irr*, and we include outputs of this ESM in the analysis as in the year 1901, irrigated fraction is very limited (Figure A1a). The land-use map and time-series data used in these simulations are from the Land-Use Harmonization phase 2 project (LUH2[47]), in which all crop management activities-related data, including irrigated land distribution, is obtained from the History Database of the Global Environment 3.2 (HYDE 3.2)[57]. The irrigated land data from HYDE 3.2 during the period 1901-2014 has two sources: for the

period pre-1960, the data is directly collected from FAO[58], and for the post-1960 period, the numbers are calculated by multiplying the term "area equipped for irrigation" in FAO statistics by the fraction of actual irrigated area in area equipped for irrigation from Global Map of Irrigation Areas version 5 (GMIA_v5)[59].

Climate extremes Most models report output variables at the 3-hourly frequency to enable analysis of sub-daily extremes, but CNRM-CM6-1 only provides daily mean, maximum, and minimum values, so we calculate several moist-heat metrics based on daily maximum temperature and minimum air relative humidity to calculate the maximum metrics consistent with a previous study[60], thereby assuming that the lowest relative humidity occurs when the temperature is maximum.

HUMIDEX (HU) is a feel-like heat stress metric developed in the late 1970s, and it was first used for the meteorological service in Canada[61]. It is calculated as:

$$\mathrm{HU} = T_{\mathrm{C}} + \frac{5}{9}\left(\frac{e_{\mathrm{RH}}}{100} - 10\right)$$

where T_C is the temperature at 2-meter height (°C), e_{RH} (Pa) is the vapour pressure calculated based on relative humidity (RH) and saturated vapour pressure (e_s in Pa):

$$e_{\mathrm{RH}} = \mathrm{RH}e_{\mathrm{s}},$$

HU is still used by the Canadian Centre for Occupational Health and Safety (CCOHS) to inform the general public if the weather conditions may be comfortable based on the following thresholds: 20-29, 30-39, 40-45, and over 46 represent the warning of 'little discomfort', 'some discomfort', 'great discomfort', and 'dangerous', respectively[62].

T_w is a measure of heat stress considering the maximum potential evaporative cooling impact[63]. It can be measured by a thermometer covered in water-soaked cloth over which air is passed[64]. The calculation of T_w is very computationally expensive, so we employ a simplified method[28]:

$$\begin{aligned} T_{\mathrm{W}} = {} & T_{\mathrm{C}} \arctan(0.151977\sqrt{\mathrm{RH} + 8.313659}) \\ & + \arctan\left(T_{\mathrm{C}} + \mathrm{RH}\right) - \arctan(\mathrm{RH} - 1.676331) \\ & + 0.00391838\mathrm{RH}^{3/2} \arctan(0.023101RH) - 4.68035 \end{aligned}$$

Based on previous studies[63,65], when T_w is over 31 °C, physical labour becomes impossible, and exposure to T_w exceeding 35 °C for more than 6 hours is dangerous even for healthy individuals. However, the maximum evaporative cooling (swamp cooler) is not easy to approach, as in previous heatwave events, high casualties already existed even if the T_w is less than 28 °C[66]. Other metrics are described in Supplementary Note 3.

Data processing Outputs from E3SM, IPSL-CM6, and CNRM-CM6-1 are firstly regridded to the resolution of CESM2, CESM_gw ($0.9° \times 1.25°$), and then the moist-heat metrics are calculated. After calculating the moist-heat metrics, we further processed the results to separate the impacts of irrigation expansion from other forcings. We first calculated irrigation expansion's impacts on the absolute values of extreme events as well as surface energy fluxes. We select two periods, the first 30 years (1901-1930) and the last 30 years (1985-2014), for both simulations (*tranirr* and *1901irr*) to calculate the impacts of all forcings, all forcings except irrigation expansion, and irrigation expansion, on near-surface climate (see Table 1). For the *tranirr* simulations, we assume that the difference between the results during the two periods is the consequence of all forcings. Similarly, the difference between the results during the two periods for the *1901irr* simulations is assumed to be the consequence of other forcings. The difference between these two simulations during the 1985-2014 period is assumed to represent the impacts of irrigation expansion as the only difference between them is whether irrigation extent is transient.

Apart from the absolute value of extreme events, we also calculate the probability ratio (PR) for several extreme events, which has been used in previous studies to show the changes in climate extreme events frequency[13,67]. The extreme events defined in this study are based on percentile values, e.g., a 99^{th} percentile event means that in the reference period, it happens once per 100 time steps (3 hours per 300 hours for 3-hourly outputs), or in other words, it indicates the 1% time steps with the most extreme values. Considering that outputs from CNRM-CM6-1 is at a daily frequency, we select the 92^{th}, 96^{th}, and 99.2^{th} percentile events for this ESMs to represent the 99^{th}, 99.5^{th}, and 99.9^{th} percentile events simulated by other ESMs. This is based on an assumption that those extreme events calculated based on maximum temperature and minimum humidity last 3 hours during the day, so a 92^{th} percentile value means 8 days per 100 days and then 24 hours per 2400 hours, which is equal to 3 hours per 300 hours for 3-hourly outputs. The PR is calculated as:

$$PR = \frac{P_{new}(X_{ext})}{P_{ref}(X_{ext})},$$

where $P_{new}(X_{ext})$ is the probability of a certain kind of extreme event (X_{ext}) during the new exp_period and $P_{ref}(X_{ext})$ is the probability of the same kind of event during the reference exp_period. Let us assume, for example, that the 99^{th} percentile value of T_{2m} is 33 °C in the reference exp_period, meaning the extreme events are the ones with $T_{2m} > 33$ °C: if the frequency of these events is 4% in the new exp_period, then the PR is 4. Thus, a PR of more than 1 indicates that this event occurs more frequently in the new exp_period compared to the reference exp_period, and vice versa. Similar to absolute values, we also select two periods (1901-1930 and 1985-2014) for both *tranirr* and *1901irr*, then calculate the PR between them for the 99.0^{th}, 99.5^{th}, and 99.9^{th} percentile events for T_{2m}, HU, and T_w. To further investigate the temporal trend of irrigation expansion's impacts, we calculated the mean value of annual hours exposed to warm extremes for four groups of grid cells, with irrigation expansion of 0%

- 20%, 20% - 30%, 30% - 40%, and more than 40%.

Data Availability

Code Availability

References

[1] Döll, P., Fiedler, K. & Zhang, J. Global-scale analysis of river flow alterations due to water withdrawals and reservoirs. *Hydrology And Earth System Sciences*. **13**, 2413-2432 (2009)

[2] Tatsumi, K. & Yamashiki, Y. Effect of irrigation water withdrawals on water and energy balance in the Mekong River Basin using an improved VIC land surface model with fewer calibration parameters. *Agricultural Water Management*. **159** pp. 92-106 (2015)

[3] Zhu, B., Huang, M., Cheng, Y., Xie, X., Liu, Y., Zhang, X., Bisht, G., Chen, X., Missik, J. & Liu, H. Effects of irrigation on water, carbon, and nitrogen budgets in a semiarid watershed in the Pacific northwest: A modeling study. *Journal Of Advances In Modeling Earth Systems*. **12**, e2019MS001953 (2020)

[4] Al-Yaari, A., Ducharne, A., Thiery, W., Cheruy, F. & Lawrence, D. The role of irrigation expansion on historical climate change: insights from CMIP6. *Earth's Future*, **10**, e2022EF002859 (2022)

[5] McDermid, S., Nocco, M., Lawston-Parker, P., Keune, J., Pokhrel, Y., Jain, M., Jägermeyr, J., Brocca, L., Massari, C., Jones, A. & Others Irrigation in the Earth system. *Nature Reviews Earth & Environment*. pp. 1-19 (2023)

[6] Puma, M. & Cook, B. Effects of irrigation on global climate during the 20th century. *Journal Of Geophysical Research: Atmospheres*. **115** (2010)

[7] Cook, B., Shukla, S., Puma, M. & Nazarenko, L. Irrigation as an historical climate forcing. *Climate Dynamics*. **44** pp. 1715-1730 (2015)

[8] Kang, S. & Eltahir, E. Impact of irrigation on regional climate over Eastern China. *Geophysical Research Letters*. **46**, 5499-5505 (2019)

[9] Sacks, W., Cook, B., Buenning, N., Levis, S. & Helkowski, J. Effects of global irrigation on the near-surface climate. *Climate Dynamics*. **33** pp. 159-175 (2009)

[10] Thiery, W., Davin, E., Lawrence, D., Hirsch, A., Hauser, M. & Seneviratne, S. Present-day irrigation mitigates heat extremes. *Journal Of Geophysical Research: Atmospheres*. **122**, 1403-1422 (2017)

[11] Li, X., Li, X., Hua, W., Ma, H., Zhou, J. & Pang, X. Modeling the effects of present-day irrigation on temperature extremes over China. *Frontiers In Earth Science*. **11** pp. 1084892 (2023)

[12] Huang, X. & Ullrich, P. Irrigation impacts on California's climate with the variable-resolution CESM. *Journal Of Advances In Modeling Earth Systems*. **8**, 1151-1163 (2016)

[13] Thiery, W., Visser, A., Fischer, E., Hauser, M., Hirsch, A., Lawrence, D., Lejeune, Q., Davin, E. & Seneviratne, S. Warming of hot extremes alleviated by expanding irrigation. *Nature Communications*. **11**, 290 (2020)

[14] Hirsch, A., Wilhelm, M., Davin, E., Thiery, W. & Seneviratne, S. Can climate-effective land management reduce regional warming?. *Journal Of Geophysical Research: Atmospheres*. **122**, 2269-2288 (2017)

[15] Kala, J., Valmassoi, A. & Hirsch, A. Assessing the maximum potential cooling benefits of irrigation in Australia during the "Angry Summer" of 2012/2013. *Weather And Climate Extremes*. **39** pp. 100538 (2023)

[16] Cramer, M. & Jay, O. Biophysical aspects of human thermoregulation during heat stress. *Autonomic Neuroscience*. **196** pp. 3-13 (2016)

[17] Buzan, J. & Huber, M. Moist heat stress on a hotter Earth. *Annual Review Of Earth And Planetary Sciences*. **48** pp. 623-655 (2020)

[18] Givoni, B. & Belding, H. The cooling efficiency of sweat evaporation. *Biometeorology*. pp. 304-314 (1962)

[19] Sorooshian, S., Li, J., Hsu, K. & Gao, X. How significant is the impact of irrigation on the local hydroclimate in California's Central Valley? Comparison of model results with ground and remote-sensing data. *Journal Of Geophysical Research: Atmospheres*. **116** (2011)

[20] Lee, E., Sacks, W., Chase, T. & Foley, J. Simulated impacts of irrigation on the atmospheric circulation over Asia. *Journal Of Geophysical Research: Atmospheres*. **116** (2011)

[21] Buzan, J., Oleson, K. & Huber, M. Implementation and comparison of a suite of heat stress metrics within the Community Land Model version 4.5. *Geoscientific Model Development*. **8**, 151-170 (2015)

[22] Zhao, Y., Ducharne, A., Sultan, B., Braconnot & P. Vautard, R. Estimating heat stress from climate-based indicators: present-day biases and future spreads in the CMIP5 global climate model ensemble. *Environmental Research Letters*, **10**, 084013 (2015)

[23] Mishra, V., Ambika, A., Asoka, A., Aadhar, S., Buzan, J., Kumar, R. & Huber, M. Moist heat stress extremes in India enhanced by irrigation. *Nature Geoscience*. **13**, 722-728 (2020)

[24] Krakauer, N., Cook, B. & Puma, M. Effect of irrigation on humid heat extremes. *Environmental Research Letters*. **15**, 094010 (2020)

[25] Gates, W., Boyle, J., Covey, C., Dease, C., Doutriaux, C., Drach, R., Fiorino, M., Gleckler, P., Hnilo, J., Marlais, S. & Others An overview of the results of the Atmospheric Model Intercomparison Project (AMIP I). *Bulletin Of The American Meteorological Society*. **80**, 29-56 (1999)

[26] Li, J., Han, Z. & Xie, Z. Model analysis of long-term trends of aerosol concentrations and direct radiative forcings over East Asia. *Tellus B: Chemical And Physical Meteorology*. **65**, 20410 (2013)

[27] Babu, S., Manoj, M., Moorthy, K., Gogoi, M., Nair, V., Kompalli, S., Satheesh, S., Niranjan, K., Ramagopal, K., Bhuyan, P. & Others Trends in aerosol optical depth over Indian region: Potential causes and impact indicators. *Journal Of Geophysical Research: Atmospheres*. **118**, 11-794 (2013)

[28] Stull, R. Wet-bulb temperature from relative humidity and air temperature. *Journal Of Applied Meteorology And Climatology*. **50**, 2267-2269 (2011)

[29] Jha, R., Mondal, A., Devanand, A., Roxy, M. & Ghosh, S. Limited influence of irrigation on pre-monsoon heat stress in the Indo-Gangetic Plain. *Nature Communications*. **13**, 4275 (2022)

[30] Chiang, F., Cook, B. & McDermid, S. Diverging global dry and humid heat responses to modern irrigation. *Earth Interactions*. **27**, e230006 (2023)

[31] Yao, Y., Vanderkelen, I., Lombardozzi, D., Swenson, S., Lawrence, D., Jägermeyr, J., Grant, L. & Thiery, W. Implementation and evaluation of irrigation techniques in the community land model. (Fort Collins, Colo.:[Verlag nicht ermittelbar],2022)

[32] De Hertog, S., Havermann, F., Vanderkelen, I., Guo, S., Luo, F., Manola, I., Coumou, D., Davin, E., Duveiller, G., Lejeune, Q. & Others The biogeophysical effects of idealized land cover and land management changes in Earth system models. *Earth System Dynamics*. **14**, 629-667 (2023)

[33] Ambika, A. & Mishra, V. Improved water savings and reduction in moist heat stress caused by efficient irrigation. *Earth's Future*. **10**, e2021EF002642 (2022)

[34] Alexandratos, N. & Bruinsma, J. World agriculture towards 2030/2050: the 2012 revision. (2012)

[35] Leng, G., Huang, M., Tang, Q. & Leung, L. A modeling study of irrigation effects on global surface water and groundwater resources under a changing climate. *Journal Of Advances In Modeling Earth Systems*. **7**, 1285-1304 (2015)

[36] Zhou, T., Leung, L. R., Leng, G., Voisin, N., Li, H. Y., Craig, A. P., Tesfa, T., Mao, Y. Global Irrigation Characteristics and Effects Simulated by Fully Coupled Land Surface, River, and Water Management Models in E3SM. *Journal of Advances in Modeling Earth Systems*. **12**(10) (2020)

[37] Wisser, D., Fekete, B., Vörösmarty, C. & Schumann, A. Reconstructing 20th century global hydrography: a contribution to the Global Terrestrial Network-Hydrology (GTN-H). *Hydrology And Earth System Sciences*. **14**, 1-24 (2010)

[38] Decharme, B., Costantini, M., Colin, J. A simple Approach to Represent Irrigation Water Withdrawals in Earth System Models *Journal of Advances in Modeling Earth Systems*. Under review (2024)

[39] Arboleda-Obando, P. F., Ducharne, A., Yin, Z., Ciais, P. Validation of a new global irrigation scheme in the land surface model ORCHIDEE v2. 2. *Geoscientific Model Development*. **17**, 2141-2164 (2024)

[40] Li, Y., Guan, K., Peng, B., Franz, T., Wardlow, B. & Pan, M. Quantifying irrigation cooling benefits to maize yield in the US Midwest. *Global Change Biology*. **26**, 3065-3078 (2020)

[41] Orlov, A., De Hertog, S., Havermann, F., Guo, S., Luo, F., Manola, I., Thiery, W., Lejeune, Q., Pongratz, J., Humpenöder, F. & Others Changes in land cover and management affect heat stress and labor capacity. *Earth's Future*. **11**, e2022EF002909 (2023)

[42] De Hertog, S., Orlov, A., Havermann, F., Guo, S., Manola, I., Pongratz, J., Lejeune, Q., Schleussner, C., Menke, I., Humpenöder, F. & Others Limited effect of future land-use changes on human heat stress and labour capacity. *Authorea Preprints*. (2024)

[43] Vecellio, D., Kong, Q., Kenney, W. & Huber, M. Greatly enhanced risk to humans as a consequence of empirically determined lower moist heat stress tolerance. *Proceedings Of The National Academy Of Sciences*. **120**, e2305427120 (2023)

[44] Guo, Q., Zhou, X., Satoh, Y. & Oki, T. Irrigated cropland expansion exacerbates the urban moist heat stress in northern India. *Environmental Research Letters*. **17**, 054013 (2022)

[45] Williams, Ian N and Pierrehumbert, Raymond T and Huber, Matthew. Global warming, convective threshold and false thermostats. *Geophysical Research Letters*. **21** pp. L21805 (2009)

[46] Williams, I. & Pierrehumbert, R. Observational evidence against strongly stabilizing tropical cloud feedbacks. *Geophysical Research Letters*. **44**, 1503-1510 (2017)

[47] Hurtt, G., Chini, L., Sahajpal, R., Frolking, S., Bodirsky, B., Calvin, K., Doelman, J., Fisk, J., Fujimori, S., Klein Goldewijk, K. & Others Harmonization of global land use change and management for the period 850–2100 (LUH2) for CMIP6. *Geoscientific Model Development*. **13**, 5425-5464 (2020)

[48] Iturbide, M., Gutiérrez, J., Alves, L., Bedia, J., Cerezo-Mota, R., Cimadevilla, E., Cofiño, A., Di Luca, A., Faria, S., Gorodetskaya, I. & Others An update of IPCC climate reference regions for subcontinental analysis of climate model data: definition and aggregated datasets. *Earth System Science Data*. **12**, 2959-2970 (2020)

[49] Savitzky, A. & Golay, M. Smoothing and differentiation of data by simplified least squares procedures.. *Analytical Chemistry*. **36**, 1627-1639 (1964)

[50] Danabasoglu, G., Lamarque, J., Bacmeister, J., Bailey, D., DuVivier, A., Edwards, J., Emmons, L., Fasullo, J., Garcia, R., Gettelman, A. & Others The community earth system model version 2 (CESM2). *Journal Of Advances In Modeling Earth Systems*. **12**, e2019MS001916 (2020)

[51] Boucher, O., Servonnat, J., and others. Presentation and evaluation of the IPSL-CM6A-LR climate model. *Journal of Advances in Modeling Earth Systems*. **12**, e2019MS002010 (2020).

[52] Seland, Ø., Bentsen, M., Olivié, D., Toniazzo, T., Gjermundsen, A., Graff, L., Debernard, J., Gupta, A., He, Y., Kirkevåg, A. & Others Overview of the Norwegian Earth System Model (NorESM2) and key climate response of CMIP6 DECK, historical, and scenario simulations. *Geoscientific Model Development*. **13**, 6165-6200 (2020)

[53] Golaz, J. C., Van Roekel, L. P., Zheng, X., Roberts, A. F., Wolfe, J. D., Lin, W., Bradley, A. M., Tang, Q., Maltrud, M. E., Forsyth, R. M., Zhang, C., Zhou, T., Zhang, K., Zender, C. S., Wu, M., Wang, H., Turner, A. K., Singh, B., Richter, J. H., . . . Bader, D. C. The DOE E3SM Model Version 2: Overview of the Physical Model and Initial Model Evaluation.*Journal of Advances in Modeling Earth Systems*. **14**(12) (2022)

[54] Voldoire, A., Saint-Martin, D., Sénési, S., Decharme, B., Alias, A., Chevallier, M., Colin, J., Guérémy, J., Michou, M., Moine, M. & Others Evaluation of CMIP6 deck experiments with CNRM-CM6-1. *Journal Of Advances In Modeling Earth Systems*. **11**, 2177-2213 (2019)

[55] Colin, J., Decharme, B., Cattiaux, J., & Saint-Martin, D. Groundwater Feedbacks on Climate Change in the CNRM Global Climate Model. *Journal of Climate*. **36**, 7599-7617 (2023) `https://doi.org/10.1175/JCLI-D-22-0767.1`

[56] Eyring, V., Bony, S., Meehl, G., Senior, C., Stevens, B., Stouffer, R. & Taylor, K. Overview of the Coupled Model Intercomparison Project Phase 6 (CMIP6) experimental design and organization. *Geoscientific Model Development*. **9**, 1937-1958 (2016)

[57] Klein Goldewijk, K., Beusen, A., Doelman, J. & Stehfest, E. Anthropogenic land use estimates for the Holocene–HYDE 3.2. *Earth System Science Data*. **9**, 927-953 (2017)

[58] Food and agriculture data. (2024,3), `https://www.fao.org/faostat/en/#home`

[59] Siebert, S., Kummu, M., Porkka, M., Döll, P., Ramankutty, N. & Scanlon, B. A global data set of the extent of irrigated land from 1900 to 2005. *Hydrology And Earth System Sciences*. **19**, 1521-1545 (2015)

[60] Dahl, K., Licker, R., Abatzoglou, J. & Declet-Barreto, J. Increased frequency of and population exposure to extreme heat index days in the United States during the 21st century. *Environmental Research Communications*. **1**, 075002 (2019)

[61] Masterton, J. & Richardson, F. Humidex: a method of quantifying human discomfort due to excessive heat and humidity. (Environment Canada, Atmospheric Environment,1979)

[62] CCOHS Humidex Rating and Work. (2023,8), https://www.ccohs.ca/oshanswers/phys_agents/humidex.html

[63] Haldane, J. The influence of high air temperatures No. I. *Epidemiology & Infection*. **5**, 494-513 (1905)

[64] Gupton.Jr, W. HVAC controls: Operation and maintenance. (CRC Press,2001)

[65] Sherwood, S. & Huber, M. An adaptability limit to climate change due to heat stress. *Proceedings Of The National Academy Of Sciences*. **107**, 9552-9555 (2010)

[66] Raymond, C., Matthews, T. & Horton, R. The emergence of heat and humidity too severe for human tolerance. *Science Advances*. **6**, eaaw1838 (2020)

[67] Yao, Y., Thiery, W. & Sterl, S. Winter is leaving: Reduced occurrence of extremely cold days in Belgium and implications for power system planning. (2020)

Appendix

A

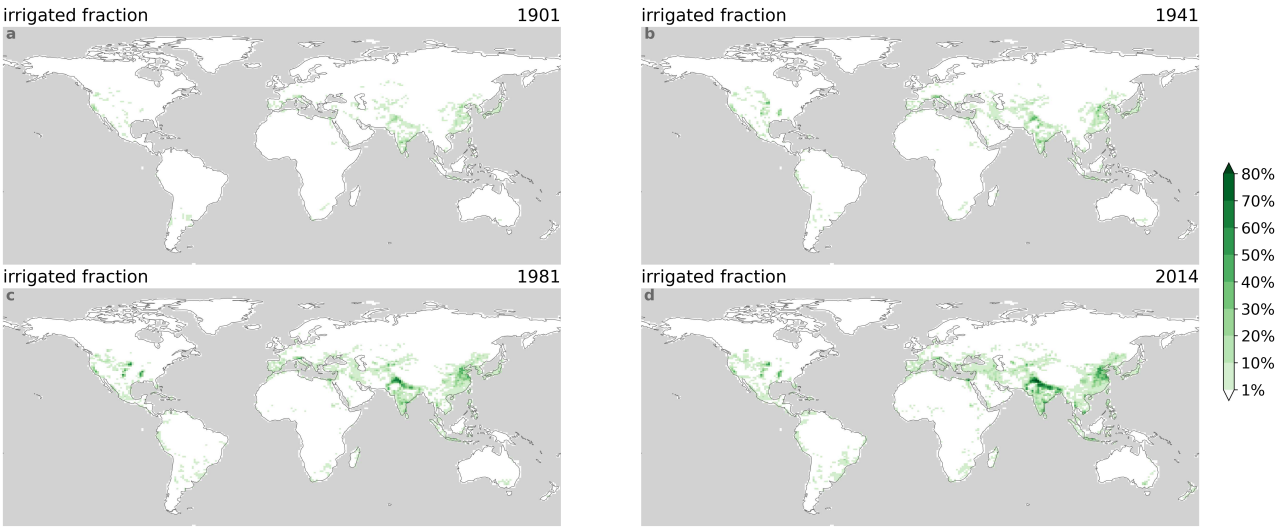

Figure A1: Irrigated fraction information is from LUH2 dataset[47]. **e** Increase in irrigated fraction between 1901 and 2014.

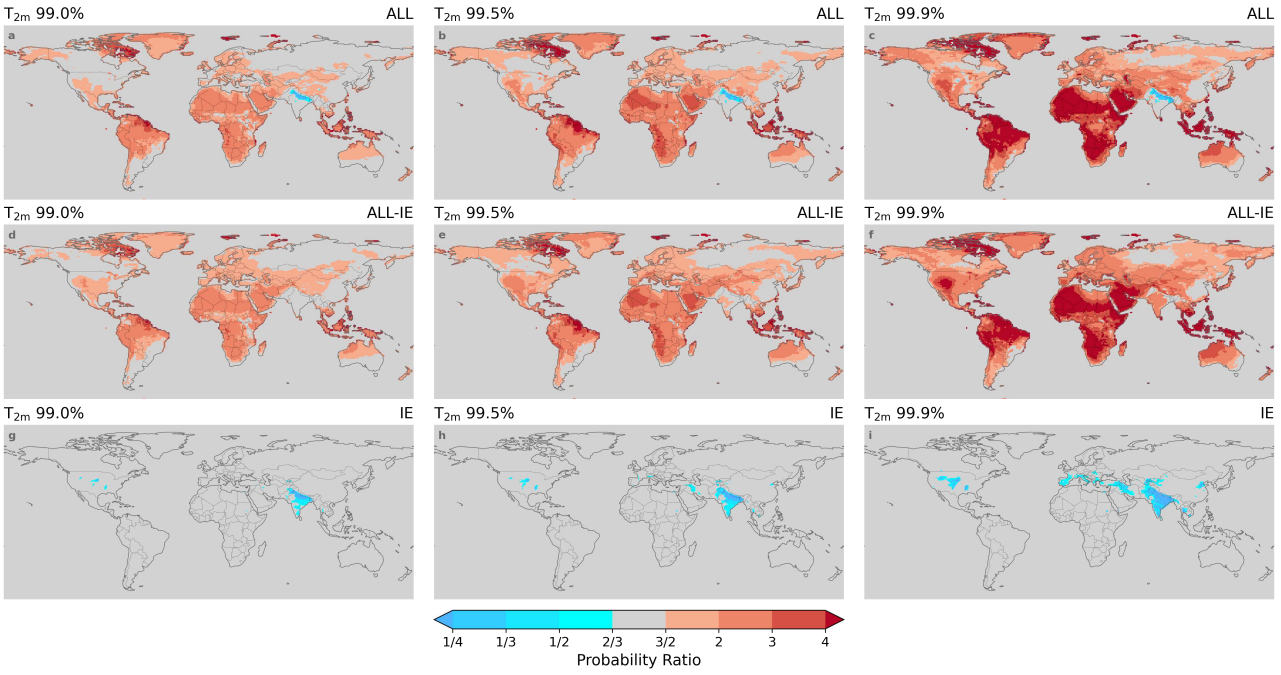

Figure A2: Similar to Figure 4 but for the 99.0^{th} (**a, d, g**), the 99.5^{th} (**b, e, h**), and the 99.9^{th} (**c, f, i**) percentile events for 2-meter air temperature T_{2m}.

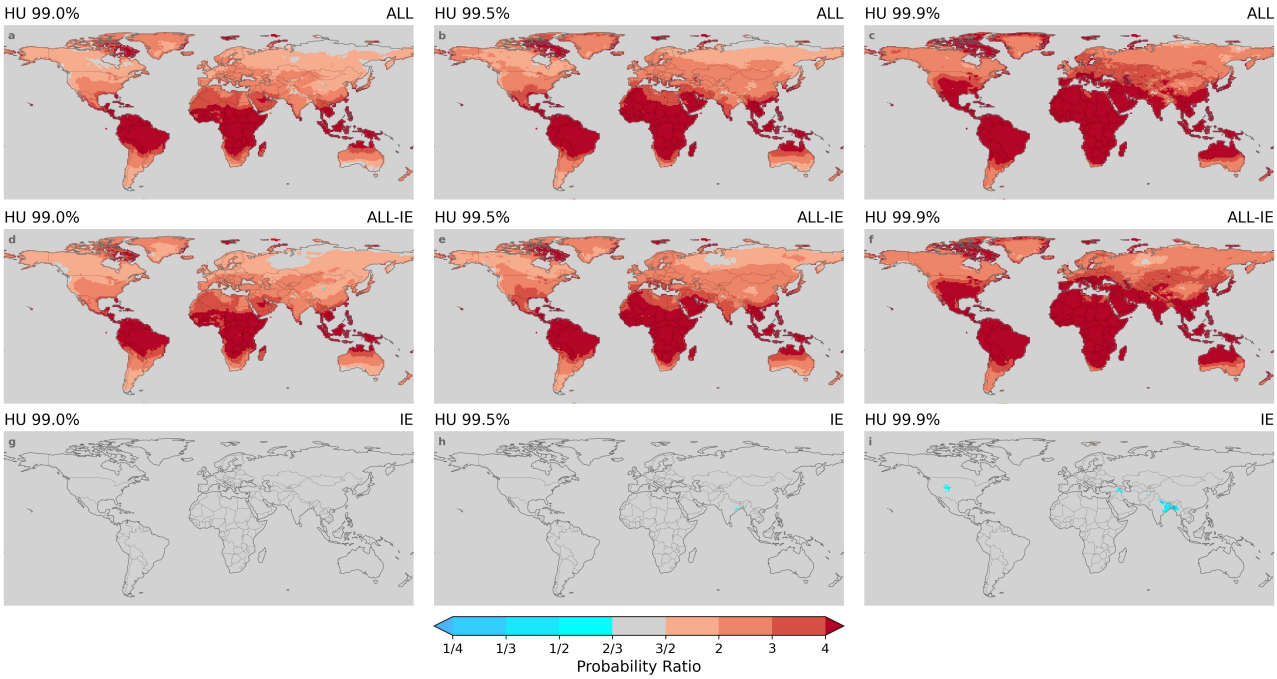

Figure A3: Same as Figure A2 but for HU.

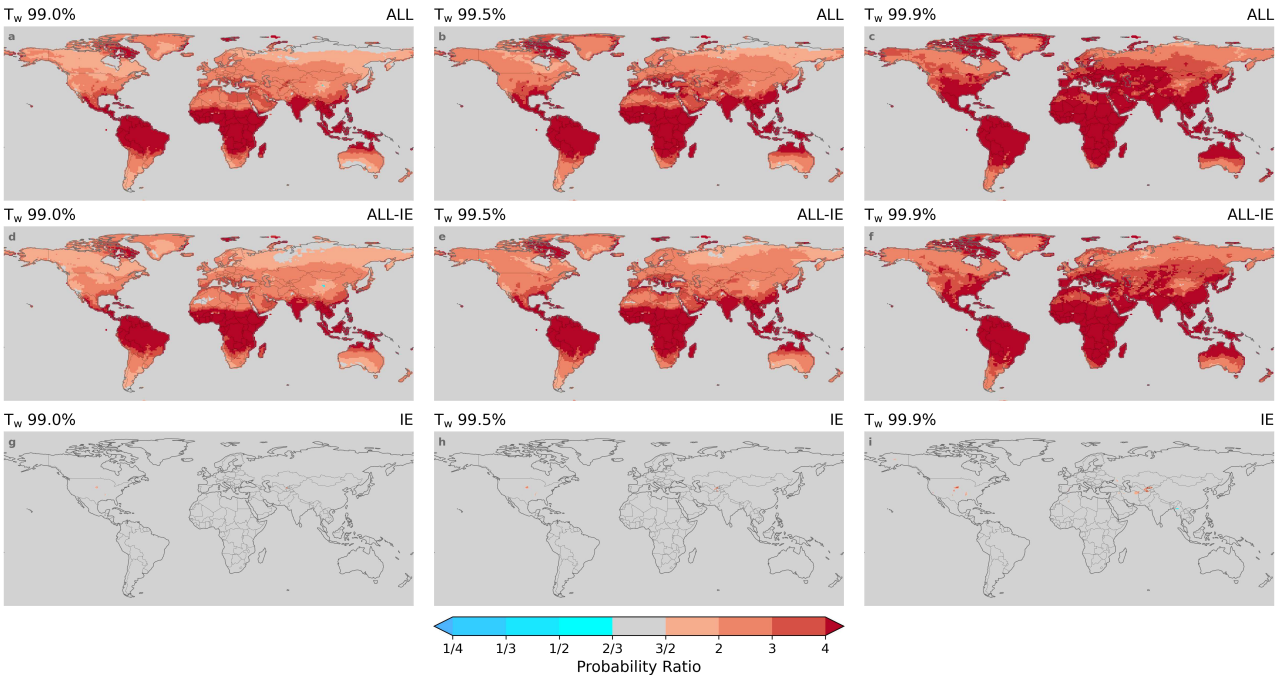

Figure A4: Same as Figure A2 but for T_w.

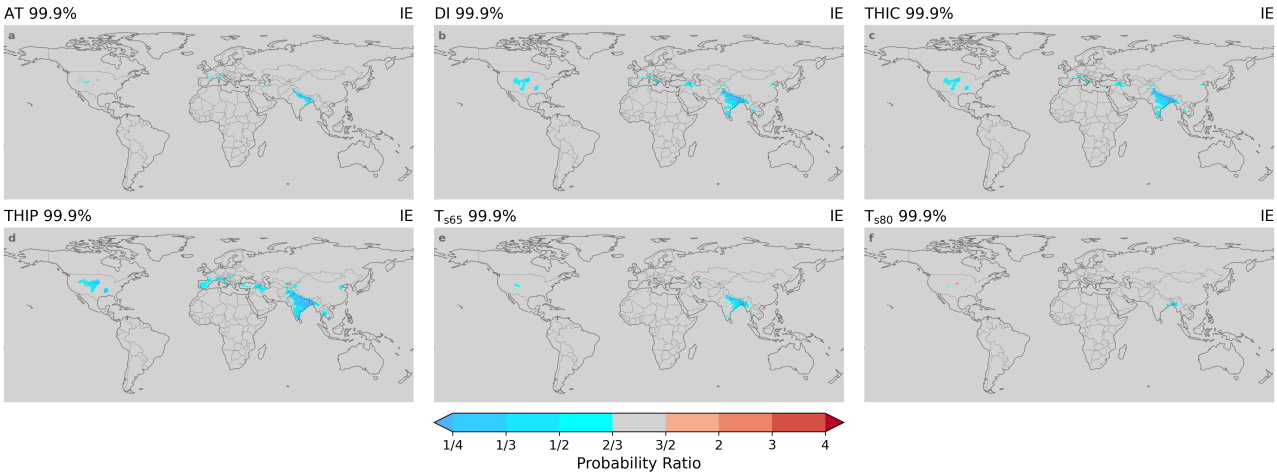

Figure A5: Similar to Figure 4 but for the 99.9^{th} percentile events for apparent temperature (AT: **a**), Discomfort Index (DI: **b**), Thermal Humidity Index for Comfort (THIC: **c**), Thermal Humidity Index for Physiology (THIP: **d**), Temperature with 65% swamp cooler (T_{s65}: **e**) and 80% swamp cooler (T_{s80}: **f**).

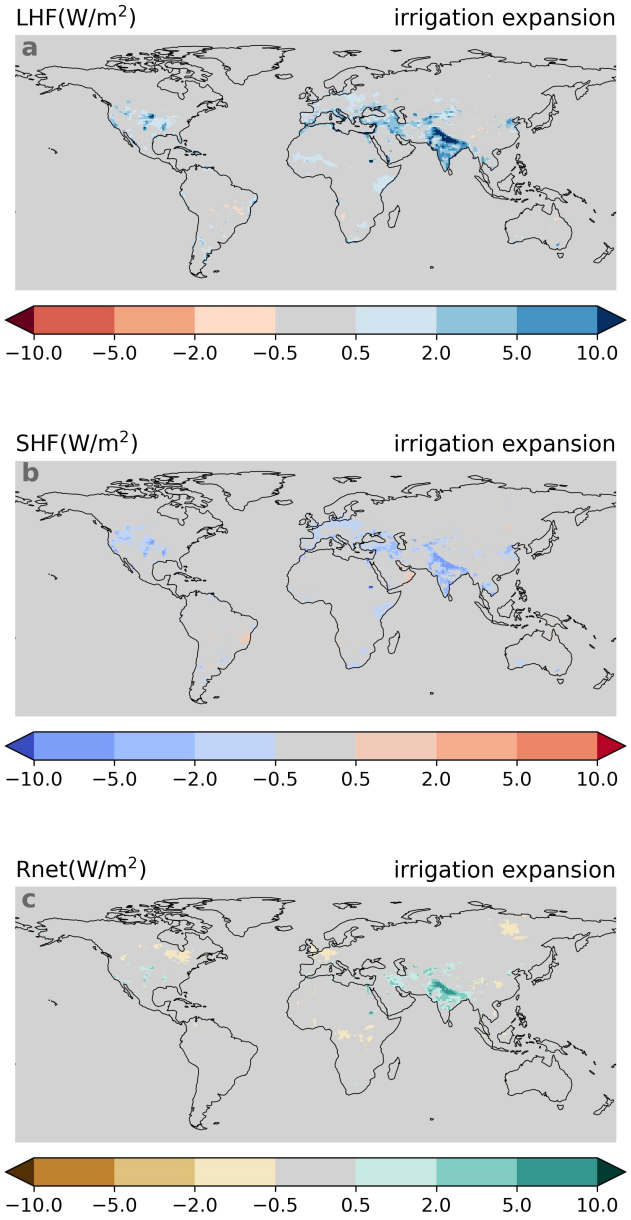

Figure A6: Impacts of irrigation expansion on latent heat flux (LHF: **a**), sensible heat flux (SHF: **b**), and net radiation (Rnet: **c**). Only signals (>0.5 or <-0.5 W/m^2) agreed by $\geq$ 4 of 6 models are shown.

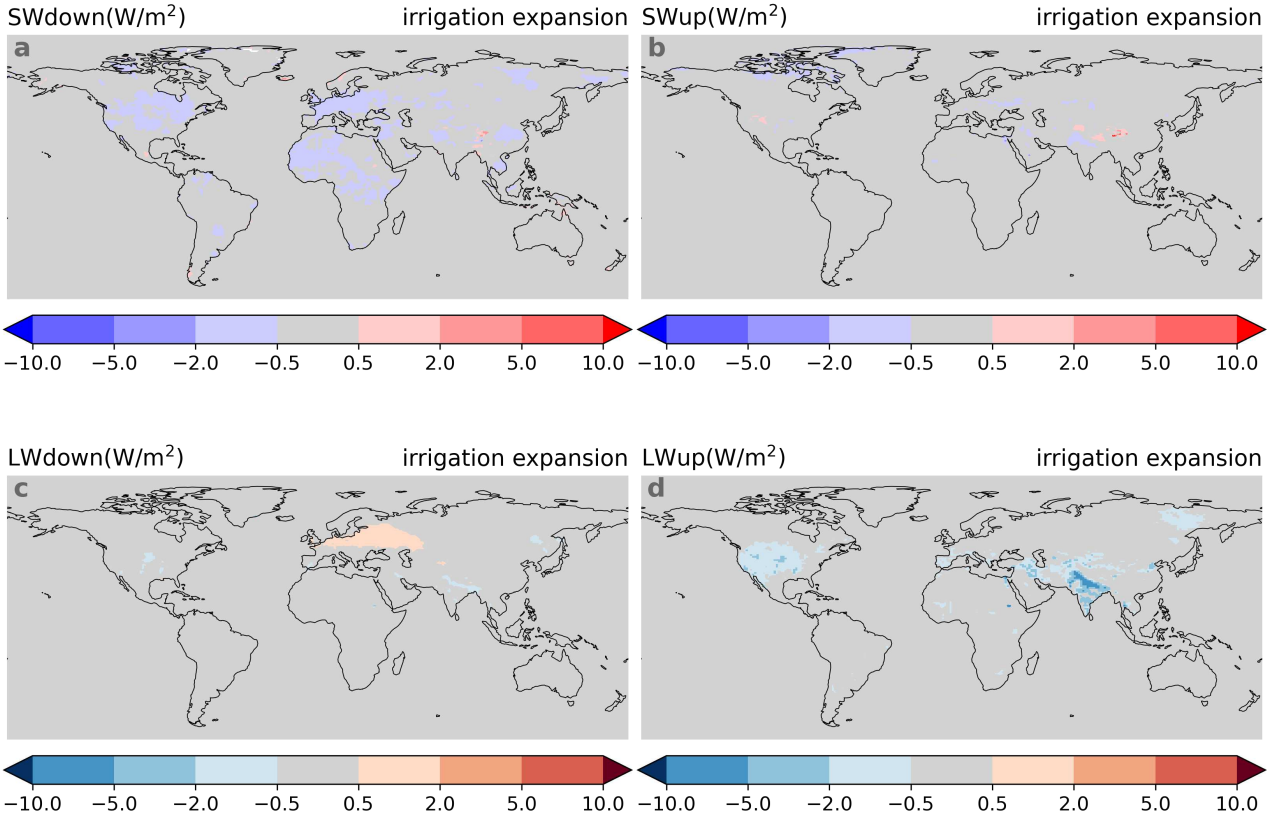

Figure A7: Same as Figure A6 but for downwelling and upwelling, short- and longwave radiation (SWdown: **a**, SWup: **b**, LWdown: **c**, and LWup: **d**.)

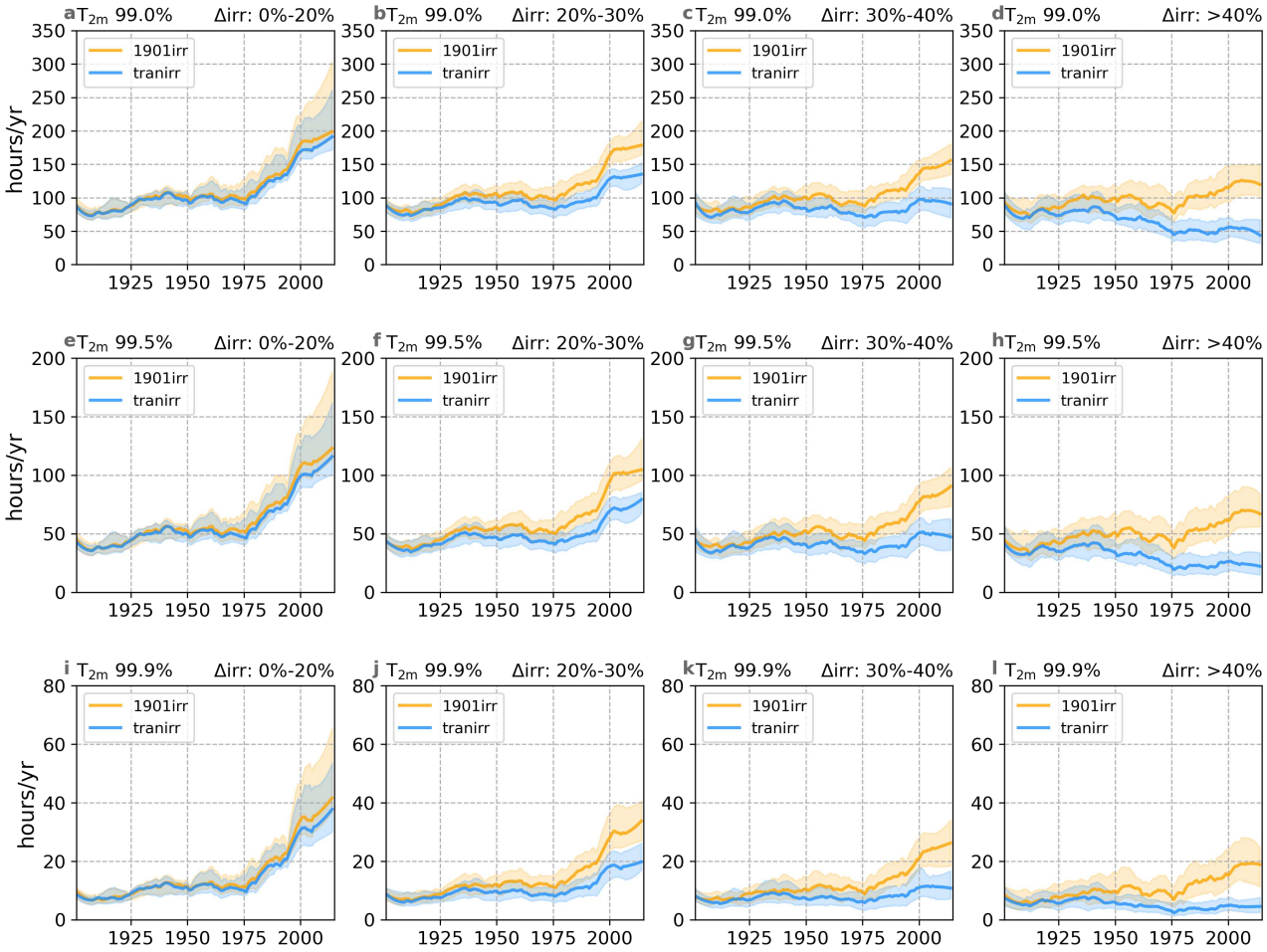

Figure A8: Similar to Figure 5 but for T_{2m} 99^{th} (**a-d**), 99.5^{th} (**e-h**), and 99.9^{th} (**i-l**) percentile extremes over grid cells with irrigation expansion of 0-20% (**a, e, i**), 20%-30% (**b, f, j**), 30%-40% (**c, g, k**) and >40% (**d, h, i**).

Supplementary Files

This is a list of supplementary files associated with this preprint. Click to download.

- SupplementaryMaterials.pdf